Journal of
Polymer Materials

Tech Science Press

https://doi.org/10.32604/jpm.2026.075026

ARTICLE

# Influence of Microstructure and Dynamic Properties on Standard Dipping Coating on Recycling Polyvinyl Alcohol Fiber/Silicon Nitride Fiber/Reduced Carbon Nano for Composite Materials

**T. Subash[1,*], M. Sekar[2] and R. Selvabharathi[3]**

[1]Department of Mechanical Engineering, PSN College of Engineering and Technology, Tirunelveli, India
[2]Department of Mechanical Engineering, AAA College of Engineering and Technology, Sivakasi, India
[3]Department of Mechanical Engineering, Renganayagi Varatharaj College of Engineering, Sivakasi, India

*Corresponding Author: T. Subash. Email: subashmat25@gmail.com

Received: 23 October 2025; Accepted: 21 January 2026; Published: 03 April 2026

**ABSTRACT:** The two distinct types of composite materials (5% to 10%) were developed using recycled polyvinyl alcohol fiber (RPA), silicon nitride fiber (SN), and reduced carbon nanoparticles (RCN). Enhanced microstructural properties and mechanical strength were attained through the application of the 3-glycidoxypropyltrimethoxysilane coupling method. The combination of the resin-like properties of RPA-SN fiber resulted in the formation of robust outer strength and a high bonding structure. RPA-RCN composite materials with a weight percentage of 10% exhibited a tensile strength of 42 MPa. In contrast, RPA-SN-RCN composite materials containing 5% to 10% demonstrated enhanced tensile, bending, and hardness properties. Pyramid structures, solid structures, and crystal phases were formed using RCN particles. The resin and silane properties on hardness were gradually 14% increasing the outside region, whereas RPA-SN-RCN (10 wt%) on average hardness were attained at 86 (Shore-D). The microstructures on RPA-RCN (5% to 10%) samples were observed solid structure, twin boundary's structure and lattice structure. The tensile strength of RPA-SN-RCN (10%) was 67.3 MPa, whereas the impact strength of RPA-RCN (10 wt%) was 53 J/mm$^2$. The scanning electron microscopies (SEM) were used to investigate the microstructure of the RPA-SN-RCN (5%) and RPA-SN-RCN (10%) composite materials, respectively.

**KEYWORDS:** Recycled polyvinyl alcohol fiber; silicon nitride fiber; reduced carbon; microstructure; mechanical properties

## 1 Introduction

The growing emphasis on sustainable development and ecological responsibility has driven increasing interest in using recycled materials in composite manufacturing [1]. The accumulation of textile, plastic, and fibre-based wastes presents severe environmental challenges, including landfill overflow and greenhouse gas emissions. To mitigate these effects, embedding recycled fibres into polymer composites offers an eco-friendly route to reduce raw material demand, lower costs, and promote circular economy principles [2,3].

Recycled polyvinyl alcohol (PVA) fibres are gaining attention for their biodegradability, strength, and recyclability [4]. When added to polymer matrices, they improve sustainability while enhancing tensile, flexural, and impact properties [5]. In cementitious composites, PVA fibres control cracks and increase ductility and fatigue resistance [6]. In polymer composites, they provide toughness, tear resistance, and cost-effective reinforcement [7]. Recently, Ram et al. [8] reported that recycled polyvinyl alcohol (PVA)

fibers exhibit tensile strength between 400–600 MPa and modulus of 12–15 GPa, with water solubility improving interfacial bonding in cementitious and polymer composites. However, recycled fibres may face issues like contamination, reduced aspect ratio, and residual material. Treatments such as washing, surface modification, coupling agents, and optimised fibre dispersion can restore performance close to virgin PVA fibres.

Silicon nitride ($Si_3N_4$) fibre as reinforcement offers significant promise due to its excellent mechanical, thermal, and chemical properties [9]. Its high tensile strength, toughness, thermal shock resistance, low thermal expansion coefficient, and stability at elevated temperatures make it suitable for composite applications under demanding conditions [10,11]. $Si_3N_4$ fibre-reinforced epoxy composites have shown improvements in hardness, tensile strength, wear resistance, and high-temperature performance. Functionalization of $Si_3N_4$ fibres has been used to improve adhesion with the polymer matrix; for instance, silane coupling agents can improve resin/fibre interface bonding, translating into enhanced load transfer and superior mechanical behaviour [12]. Recently, Kumar et al. noted that silicon nitride fibers possess high hardness (15–18 GPa) and fracture toughness of 6–8 $MPa{\cdot}m^{1/2}$, along with chemical stability and resistance to oxidation up to 1200°C, making them excellent reinforcements in structural composites [13].

Alongside fibre reinforcements, carbon-based nanomaterials, especially reduced carbon nanoparticles are increasingly being used in polymer composites to improve electrical, thermal, and tribological properties [14]. Reduced carbon nano-fillers can enhance stiffness, wear resistance, and friction performance while maintaining low density [15]. Their large surface area enables strong interfacial interactions if well dispersed, though challenges such as agglomeration, poor wetting, and stress concentration need to be considered [16,17]. In epoxy and thermoset composites, small loadings of reduced carbon nanoparticles improve conductivity and wear resistance; higher loadings can also lead to increased stiffness and thermal conductivity [18,19]. Sharma et al. demonstrated that reduced carbon nanoparticles such as reduced graphene oxide and carbon black enhance polymer matrices with tensile strength increases of 20%–35% and thermal conductivity up to 3–5 W/m·K, while also offering corrosion resistance due to high chemical inertness [20].

However, the base polymer composite properties can still be limited by surface interactions, environmental degradation, and wear when exposed to frictional or hostile environments [21]. Coating polymer composites using standard dipping, spray, or chemical vapour deposition methods has been adopted as a strategy to protect composite surfaces and improve durability [22,23]. Surface coatings can impart enhanced hardness, reduce moisture ingress, improve abrasion resistance, and extend service life while retaining the composite's bulk properties [24]. Standard dipping methods are advantageous for their simplicity, uniform coverage, and low equipment cost, but issues such as coating adhesion, thickness uniformity, and long-term durability under dynamic loads remain to be fully understood. Lee et al. highlighted that coating methods like dip-coating and plasma spraying improve wear resistance by up to 40%, hardness by 20%–25%, and reduce friction coefficient from 0.6 to 0.2, thereby extending the life of composite materials [24].

Despite notable progress in polymer composite research, a significant gap remains in the literature. Most existing studies focus either on single reinforcements or limited hybrid combinations, while the impact of coating methods, particularly standard dipping on microstructure and mechanical behaviour is rarely explored. To overcome these limitations, the present work introduces a novel composite reinforced with recycled PVA fibres, silicon nitride fibres, and reduced carbon nanoparticles, with a standard dipping coating, targeting enhanced dynamic properties and sustainable, high-performance applications.

## 2 Materials and Methods

### *2.1 Materials and Methods*

Recycled polyvinyl alcohol fiber (RPA) was utilized as the primary reinforcement, isolated from industrial-grade polymer residues and subjected to surface cleaning before drying. The reinforcing fillers comprised silicon nitride (SN) fibers and reduced carbon nanoparticles (RCN), which were procured from certified chemical suppliers. The process involved the creation of recycled polyvinyl alcohol fiber and silicon nitride fibers by first separating the fiber layer and then subjecting it to a 24-h alkali treatment, followed by drying in sunlight. RPA was chosen for its resin-like toughness and high bonding capability when integrated with nanoparticles and ceramic fibers. Silicon nitride fibers, with an average diameter of 30 nm and a density of 3.2 g/cm$^3$, offered excellent crystalline stability and hardness enhancement to the composite. Reduced carbon nanoparticles, with an average particle size of 20 nm and density of 5.22 g/cm$^3$, exhibited hexagonal lattice bonding, enabling superior outer strength and solid phase formation within the matrix. These reinforcements were blended with epoxy resin (LY556) and hardener (HY951), which served as the binding matrix. A silane coupling agent, 3-Glycidoxypropyltrimethoxysilane, in the range of 20%, was used to improve the fiber–matrix interfacial adhesion and surface bonding. In order to enhance both the outer surface layer and the inside region of the composite materials, the standard dip coating method was implemented. The implementation of the 100 dipping was carried out on the surface of the composite. To minimize voids and bubble formation, composite samples were fabricated with controlled filler contents of 5%–10% (RPA, SN, and RCN in varying proportions). Two distinct sets of composites were prepared: RPA–RCN and RPA–SN–RCN. The former enhanced tensile and impact strength, while the latter improved hardness, bending resistance, and microstructural stability. The fabricated specimens were subsequently subjected to microstructural and mechanical characterizations. The schematic representation of the current research work is depicted in the Fig. 1.

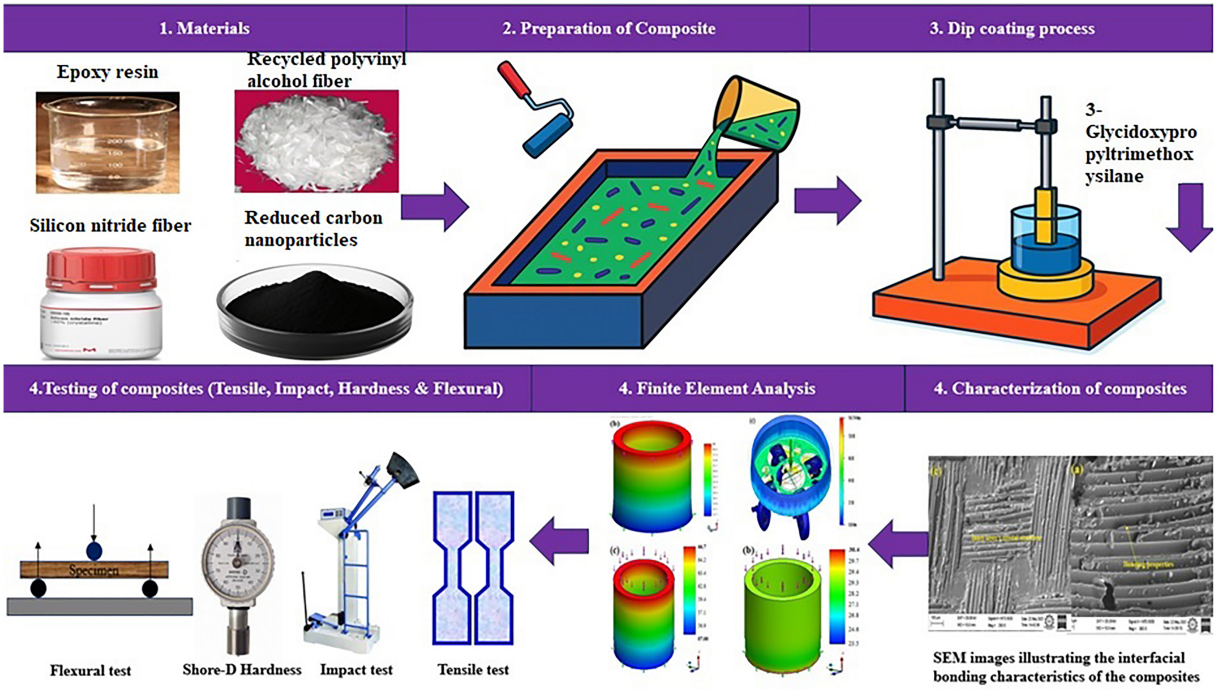


**Figure 1:** Schematic illustration of the methodology adopted in the present research work.

### *2.2 Microstructure and Mechanical Properties*

The fabricated RPA–SN–RCN and RPA–RCN nanocomposites were subjected to detailed microstructural and mechanical investigations. The detailed material composition is listed in Table 1. For microstructural observations, square samples with dimensions of 10 mm × 10 mm × 5 mm were prepared and analyzed under scanning electron microscopy (SEM) at a magnification of 500×. SEM micrographs provided insight into fiber–matrix interfacial bonding, crack propagation, and the dispersion of RCN and SN within the resin-rich regions. Distinct structural morphologies such as lattice formations, solid phases, and twin boundaries were identified, particularly in RPA–RCN (5%–10%) and RPA–SN–RCN (10%) composites, corroborating the solid phase construction described in the abstract.

**Table 1:** Specimen code and its composition.

| Specimen code | Composition code | Composition materials |
|---|---|---|
| 1. | RPA-RCN | 95%RPA-RCN (5%) |
| 2. | RPA-RCN | 90%RPA-RCN (10%) |
| 3. | SN-RCN | 95%SN-RCN (5%) |
| 4. | SN-RCN | 90%SN-RCN (10%) |
| 5. | RPA-SN-RCN | 95%RPA-SN-RCN (5%) |
| 6. | RPA-SN-RCN | 90%RPA-SN-RCN (10%) |

Mechanical testing was conducted following ASTM standards to ensure accuracy and reproducibility. Tensile strength was measured using an Instron universal testing machine at a crosshead speed of 1 mm/min. The test specimens had dimensions of 175 mm × 25 mm × 5 mm in accordance with ASTM D3039. Three-point bending tests were carried out on samples of 125 mm × 12.7 mm × 3 mm, following ASTM D790 guidelines, to evaluate flexural resistance and fracture behavior. The results indicated that higher RCN content enhanced tensile and impact strength, while SN incorporation significantly improved bending performance.

Surface hardness of the composites was evaluated using a Shore-D durometer. Measurements were taken along the outer surface layer with a dwell time of 15 s, and indentations were made at 0.50 mm intervals. The highest average hardness value, 86 Shore-D, was recorded for RPA–SN–RCN composites with 10% reinforcement, confirming the improved surface bonding and rigidity imparted by silane treatment and nanoparticle reinforcement.

## 3 Results and Discussion

### *3.1 Microstructure Studies*

As depicted in the Fig. 2, the microstructure made it evident that the RC nanoparticle and RPA fiber were directly mixed with the resin, while the outer layers' strength and bonding qualities were progressively improving [3,4]. The silane characteristics helped to strengthen the connection and prevented the inner and outer layers from developing holes, cracks, or dimples. The elongation ratio, hardness value, and microstructure of the RPA-RCN (5%) samples all abruptly increased. Better microstructure and bonding qualities were achieved by the RPA-RCN (10%) composite samples, whereas the inner layer's crystal structure, homogenous structure, and twin fiber boundaries structure all exhibited microstructure characteristics. By improving the density of the resin and silane characteristics, the SN-RCN (5%) composite material on silicon nitride fiber significantly improved the outer surface region and prevented fractures, holes,

and dimples. The inner surface layer of SN-RCN (10%) composite materials with silane characteristics showed yield strength, high hardness value, and strong bonding strength, while the microstructure made it evident that the twin boundaries structure, coarse structure, and lattice structure were present [12]. When carbon nanoparticles were directly mixed with RPA-SN-RCN (5%) composite materials, the mechanical characteristics and bonding strength were significantly amended. Better elongation ratio, yield strength, and bonding characteristics of the inner layer were achieved by RPA-SN-RCN (10%) composite materials within silane properties, while the hardness value and microstructure characteristic of the outer surface region were steadily increased by the silane process [21–23].

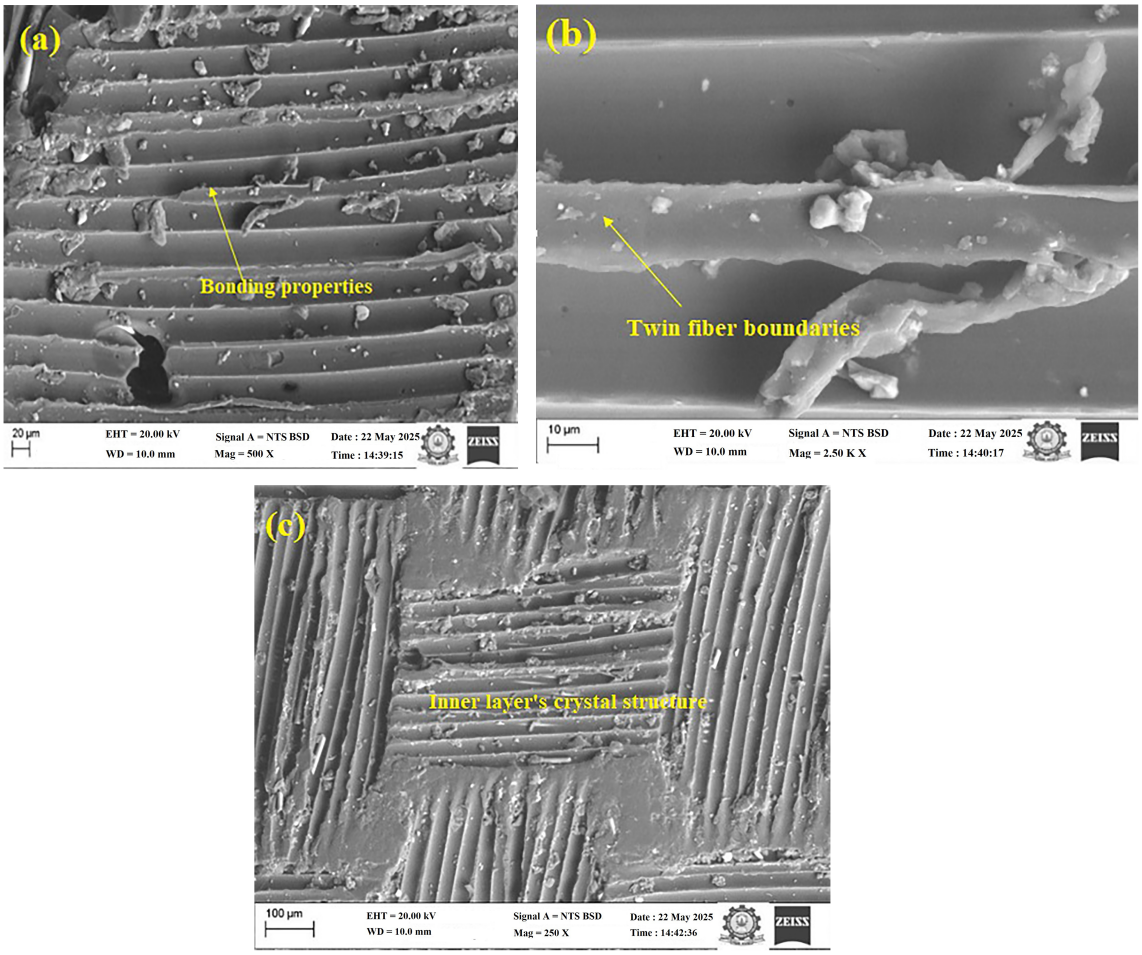


**Figure 2:** (Continued)

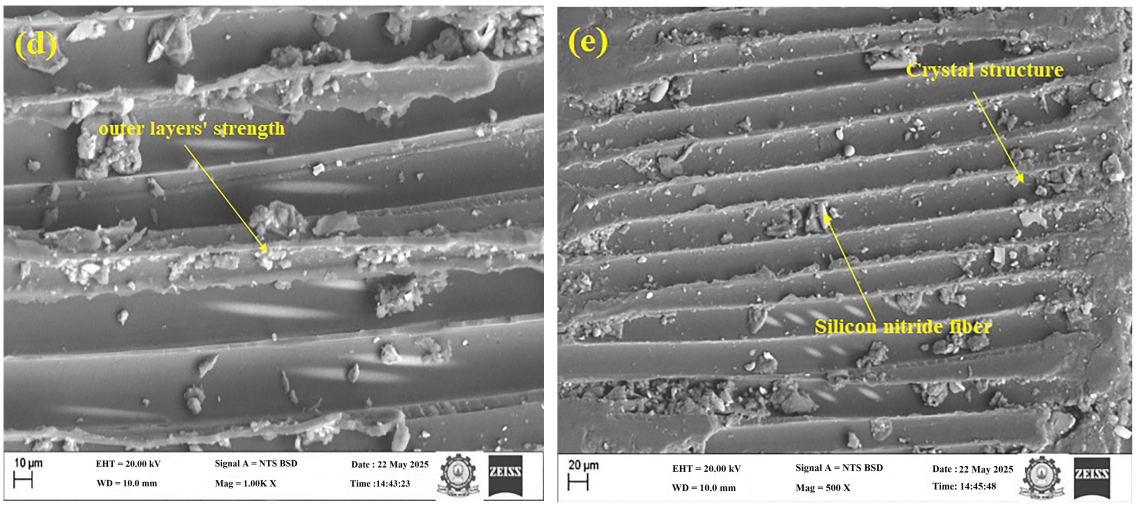


**Figure 2:** (**a**–**e**) SEM images illustrating the interfacial bonding characteristics and micro structural integrity of the fabricated RPA–SN–RCN composite materials.

### *3.2 XRD Analysis*

The XRD results distinctly demonstrated that the Recycled polyvinyl alcohol fiber (RPA) and silicon nitride (SN) fibers were predominant in the composite materials, while the RC nanoparticles contributed significantly to enhancing the microstructure and mechanical properties as shown in Fig. 3. The XRD pattern of the RPA-RCN composite materials indicated a slight increase in bonding strength and hardness values, which was evident in both the outer and inner surface regions. The XRD peaks observed for the RPA-RCN composite were (111), (200), and (222), indicating an enhancement in structural strength and mechanical properties. The XRD peak angle range for SN-RCN composite materials samples was observed between 35° and 45° angle. The (111) and (222) peaks were reinforcing the SN-RCN composite materials. The incorporation of silicon nitride fiber and reduced carbon nanoparticles exhibiting silane characteristics was enhancing the hardness value and structural integrity. The major peaks of the RPA-SN-RCN composite materials were observed at angles of 45°, 53°, and 76° in the outer surface region, with the 45° and 53° peaks being more pronounced in the RPA-SN-RCN composite. The FTIR peak locations in the RPA-SN-RCN composite materials were observed in the inner layer. The FTIR spectrum was discerned within the range of 4000 to 500 $cm^{-1}$. The fiber and nano particles was increasing the inner bonding strength and mechanical properties as shown in Fig. 3. The O-H-H stretching of bonding strength was seen at the peak position of 3737.79, while the pyramid structures and secondary's fiber were observed to reflect into the inner area at the peak positions of 1511.12 and 1338.51, respectively, as shown in Table 2. The peak position of 766.65 will enhance the homogeneous structure and increase the strength of the composite materials.

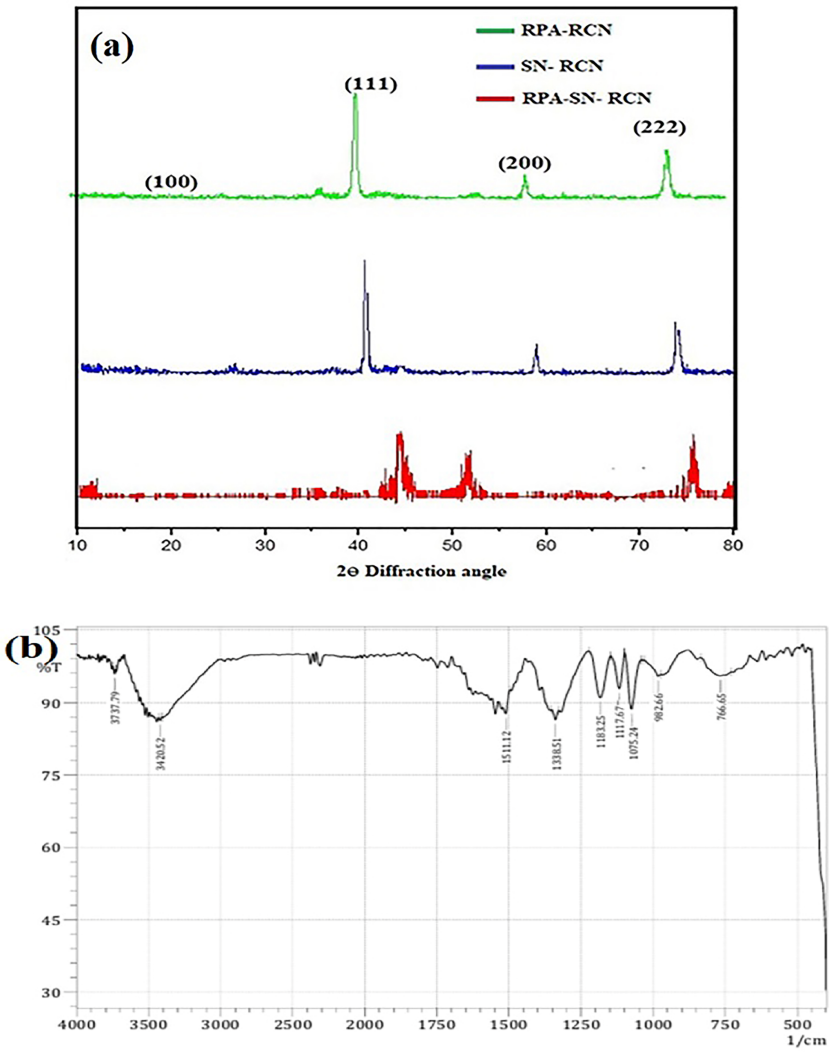


**Figure 3:** (**a**) XRD and (**b**) FTIR image of interfacial bonding characteristics and micro structural integrity of the fabricated RPA–SN–RCN composite materials.

**Table 2:** FTIR peak locations and distributions of chemical stretching.

| Peak Positions (Wave Number ($cm^{-1}$)) | Distributions |
|---|---|
| 3737.79 | O-H-H stretching of bonding strength (Fiber particle) |
| 1511.12 | CH-H stretching of pyramid structures |
| 1338.51 | OH-H stretching of secondary's fiber |
| 982.66 | C-OH stretching of crystal structure |
| 766.65 | O-CH stretching of homogenous structure |

### *3.3 Tensile Strength*

High yield strength, elongation ratio, and yield point were required to achieve the tensile strength of RPA-SN-RCN particle composite materials, whereas rapid fracture morphological growth was eminent [6,7].

The tensile strength of RPA-RCN (5%) composite materials with silane properties was 34.6 MPa, whereas the yield point and ductility strength were abruptly increased by reduced carbon nanoparticles and silane qualities as illustrated in the Fig. 4. The tensile strength of the RPA-RCN (10%) nanoparticle mix resin composite materials was 38.9 MPa. Recycling-polyvinyl alcohol fiber and silane characteristics were enhancing the inner region's primary phase and lattice structure [11–13]. The tensile strength of the SN-RCN (5%) composite materials was 35.4 MPa, while the ultimate strength, micro structure, and hardness value were enhanced by the resin, silicon nitride fiber, reduced-carbon nanoparticle, and silane characteristics. The tensile strength of the SN-RCN (10%) composite materials was 41.5 MPa, while the bonding characteristics were enhanced and silane qualities predominated on the outer surface region [19,20]. The tensile strength of the RPA-SN-RCN (5%) composite materials was 54.9 MPa, whereas the mechanical strength and outer surface region of the RCN particle, RPA fiber, and silane characteristics abruptly increased. The RPA-SN-RCN (10%) composite materials reached 62.5 MPa, while the yield strength, ultimate point, and outer surface strength increased due to the characteristics of reduced carbon nanoparticles, resin, and silane. The finite element analysis methods have been consistently applied under tensile load in the composite structure, while a mesh size of 200 was progressively divided among the larger particles and structural strength. The tensile load on composite materials reached a minimum of 33.7 MPa, and this load did not impact the structure of the outer grain boundaries, whereas 48.0 MPa on tensile load resulted in a slight collapse of the outer surface region. When the stress reached 63 MPa, the experimental and finite element results were more in line with each other. The simulation findings were directly fitted to the coarse grain boundaries structure, fine structure, and lattice structure. The RPA-SN-RCN (10%) composite materials' tensile strength, as determined by the finite element modelling approach, was 63 MPa. The bonding strength and microstructure were progressively increased by the yield strength and elongation ratio [22,23].

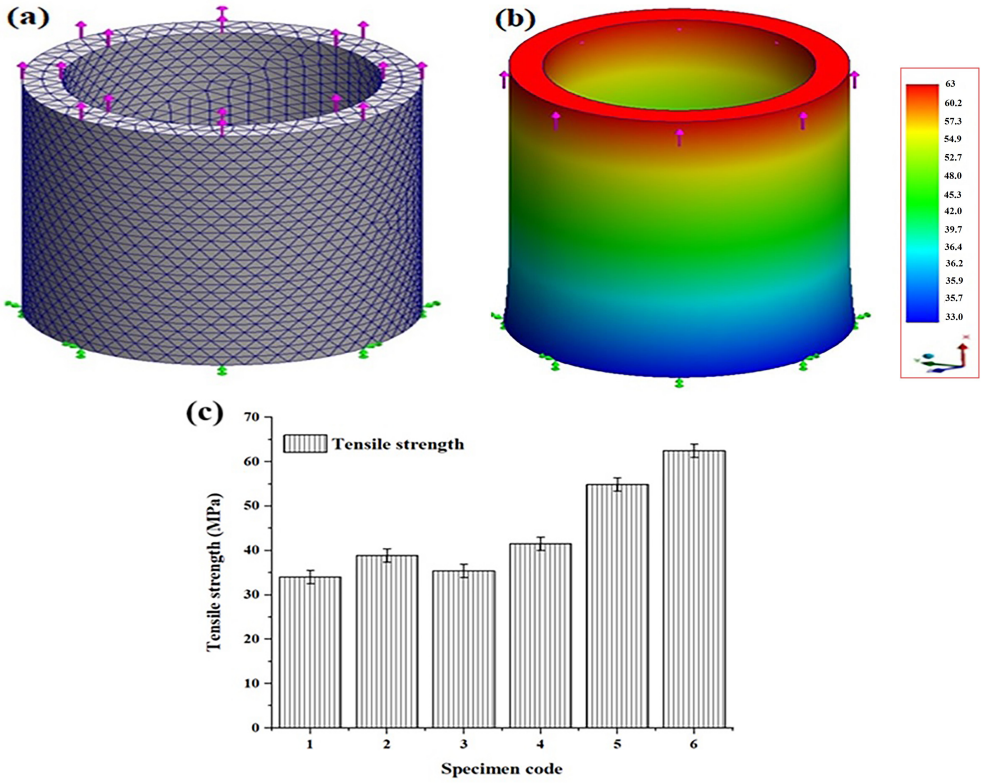


**Figure 4:** (Continued)

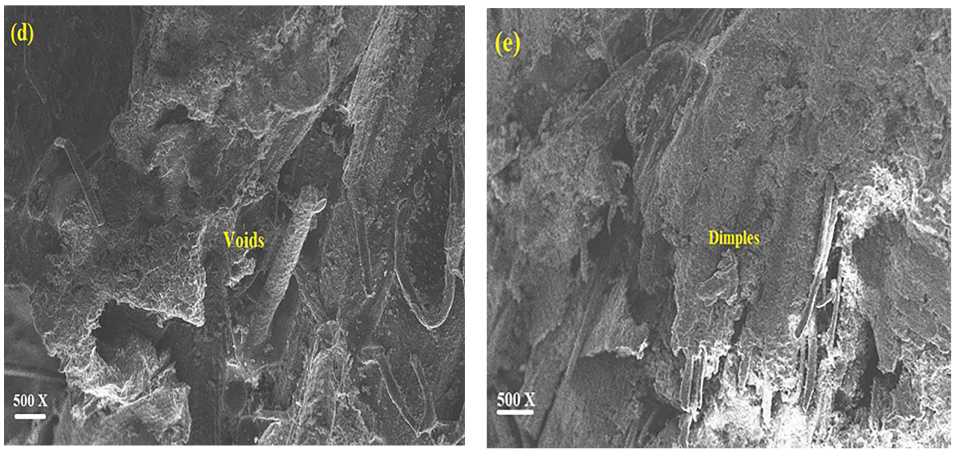


**Figure 4:** (**a**–**c**) Finite element simulation of the composite model under tensile loading, (**d**, **e**) illustrating stress distribution and correlating with the experimental results on the tensile behavior of the fabricated composites.

### *3.4 Flexible Strength*

To increase the mechanical strength and outside surface area, three-point flexible strength testing was conducted using recycled polyvinyl alcohol fiber, silicon nitride fiber, and reduced carbon nanoparticles. While recycled polyvinyl alcohol fiber and reduced carbon fiber increased bonding strength and outer surface by silane characteristics, the RPA-RCN (5%) composite materials reached 39.7 MPa for flexible strength. The elongation ratio, yield strength, and bonding properties were all steadily refining with the addition of 5% to 10% of (RCN) nanoparticles and fiber (RPA). The flexible strength of RPA-RCN (10%) composite materials was 43.2 MPa [17,18]. The silane characteristics of the SN and RCN (5%) composite materials resulted in a flexible strength of 41.3 MPa as shown in the Fig. 5. The SN fiber and RCN (10%) particle were directly supported in terms of inner bonding qualities and flexible strength. Fiber content was progressively increasing the yield strength and elongation properties; while 10% lower carbon nanoparticle and silane characteristics were boosting the strength and bonding capabilities. The SN-RCN (10%) composite material's flexible strength was attained at 44.9 MPa. The RPA-SN-RCN (5%) composite materials' flexible strength was 60.8 MPa, with the outer surface region being more dominated by RPA fiber and carbon nanoparticles. The use of finite element methods have been methodically utilized under compressive load to evaluate plastic properties, with a mesh size of 200 being progressively subdivided to accommodate larger dimensions and structural strength considerations. The flexural load applied to composite materials resulted in a minimum strength of 23.5 MPa, with no damage detected on the outer surface region or inner boundaries. A flexural load of 63.7 MPa resulted in a minor crack of both the inner and outer surface regions. The RPA-SN-RCN (10%) composite material's flexible strength was 64.6 MPa, while its hardness value, mechanical strength, and microstructure improved when compared to 5% [4,5]. In order to increase the mechanical strength and elongation ratio, the RPA and SN fiber content did not collapse the outer surface region and bonding strength. The flexural strength of RPA-SN-RCN (10%) composite materials was 66.7 MPa according to the finite element modelling method, while the flexible strength was 64.6 MPa [1].

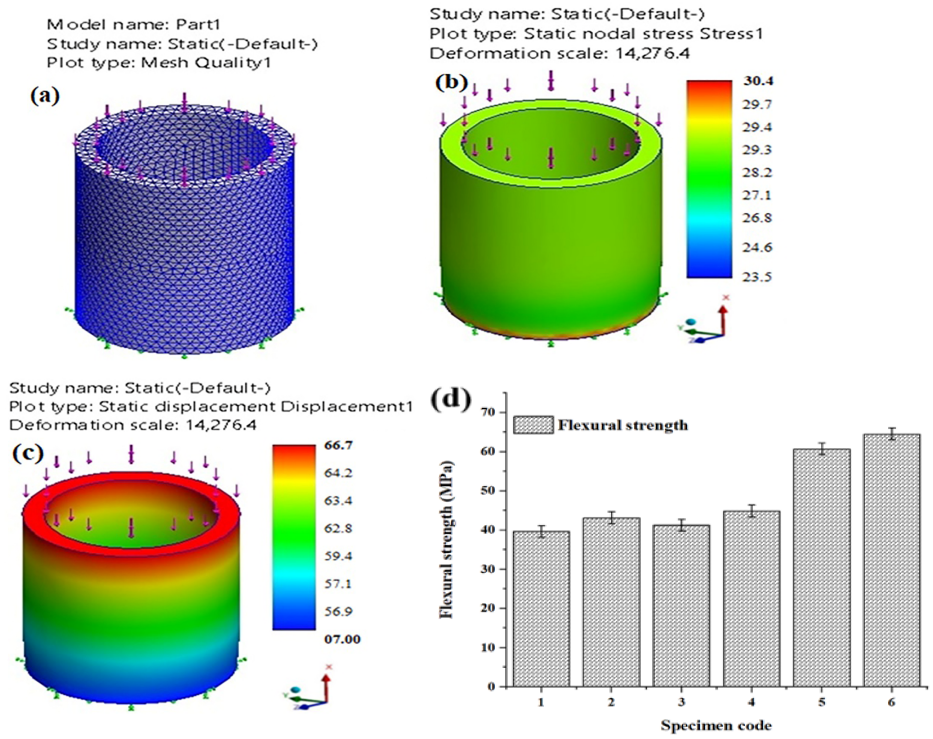


**Figure 5: (a–d)** Finite element simulation of the composite model under flexural loading, depicting stress distribution and deformation behavior consistent with experimental bending test results.

### *3.5 Impact Strength*

The bonding strength of the composite materials was strengthened by silane characteristics employing recycled polyvinyl alcohol fiber, silicon nitride fiber, and (5% to 10%) reduced carbon nanoparticles. While RPA fiber and nanoparticles were lowering the abrupt impact load, the RPA-RCN (5%) composite material achieved an impact strength of 24.7 J/m$^2$ as depicted in the Fig. 6. The RPA fiber's microstructure revealed that the outer surface region's twin boundaries, secondary structure, and primary phase had all improved [3,4]. The impact strength of the RPA-RCN (10%) composite material was 26.9 J/m$^2$, while the bonding and impact strengths increased with 10% as compared to 5% nanoparticles. SN fiber and silane characteristics were abruptly observed to have an impact strength of 26.8 J/m$^2$ for the SN-RCN (5%) composite material [3]. However, RCN nanoparticles did not sustain the inner and outer layers [19]. The impact strength of the SN-RCN (10%) composite material was 29.4 J/m$^2$, with the bonding strength, outer strength, and hardness value being increased by the SN fiber, resin, and nanoparticles [6]. The impact strength of the RPA-SN-RCN (5%) composite material was 34.7 J/m$^2$, although the secondary phase, lattice structure, and primary phase were formed by the RPA fiber, SN fiber, and RCN nanoparticle [7]. The impact strength of the RPA-SN-RCN (10%) composite materials was 37.5 J/m$^2$, while the bonding and outer strength were improved by the 10% lower carbon nanoparticle and fiber content [9].

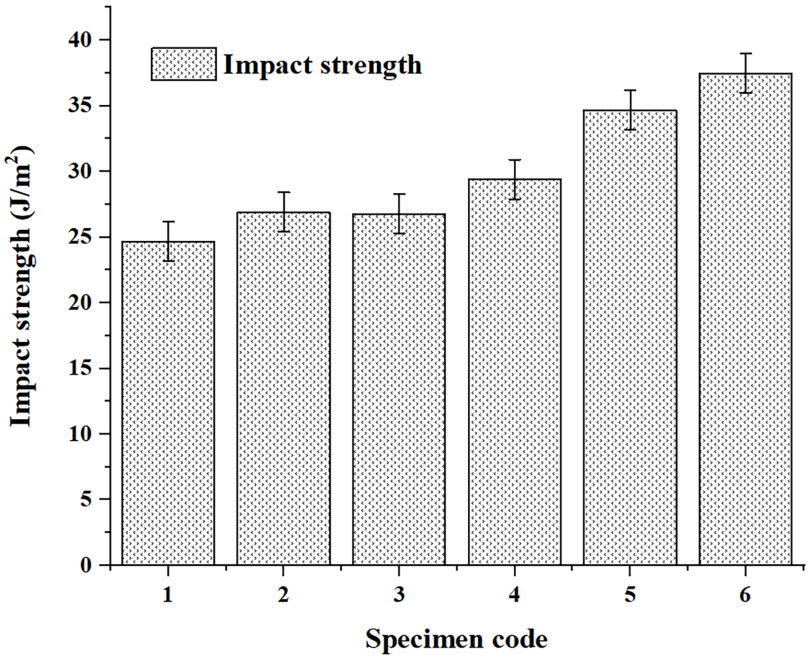


**Figure 6:** Experimental results showing the impact strength of RPA–SN–RCN composites at varying reinforcement contents.

### *3.6 Hardness Value*

The hardness value of recycled polyvinyl alcohol fiber, silicon nitride fiber, and reduced carbon nanoparticles increased as depicted in the Fig. 7. Nanoparticles increased the bonding characteristics and outer strength by 10% to 5%. The silane characteristics of the RPA-RCN (5%) composite materials were found to be improving the outer surface layer's hardness value at 64 D. The hardness values of the inner and outer surface layers were progressively raised by the 10% addition of RC nanoparticles and RPA fiber [19]. At 74 degrees, the RPA-RCN (10%) composite materials were obtained [23]. The hardness value of 68 D was evidently seen for the SN fiber, silane, and RC nanoparticles in the SN-RCN (5%) composite material. 5% of nanoparticles were directly supporting the outer surface, and the silane characteristics prevented the inner layer from cracking, getting holes, or dimpled [17]. The hardness value of the SN-RXN (10%) composite material was reached at 79 D. The lattice phase of the outer surface, bonding structure, and homogenous structure were all improved by the SN fiber on the microstructure. The RPA-SN-RCN (5%) composite material had a hardness value of 81 D, while the outer boundaries structure's microstructure and outer strength were being enhanced by RPA and SN fibers. The silane characteristics of the RPA-SN-RCN (10%) composite material led to a hardness value of 88 D. In order to directly support the outer surface region, the silane characteristics, resin, and 10% nanoparticle were enhancing the bonding strength, yield point, and elongation [24].

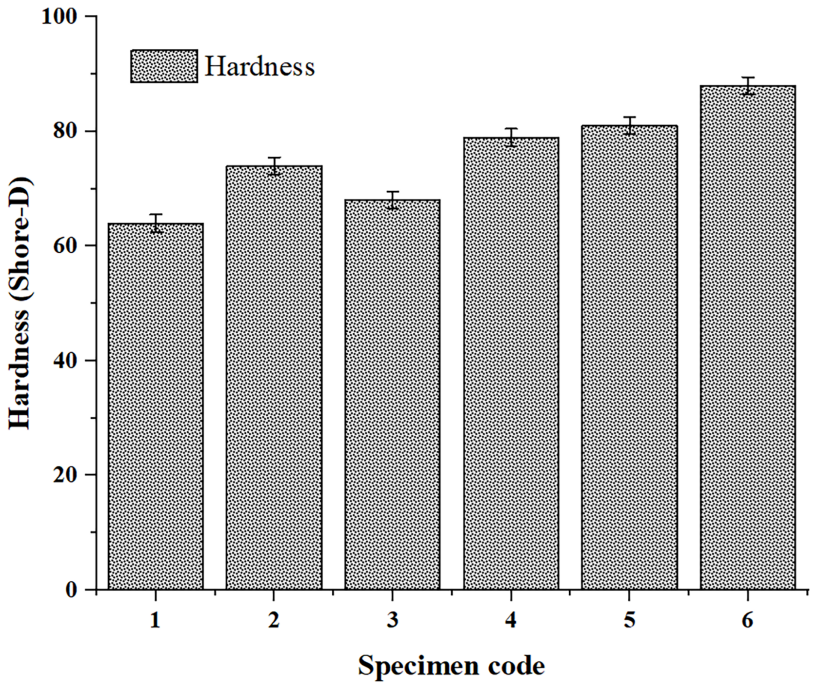


**Figure 7:** Experimental results showing the hardness value of RPA–SN–RCN composites at varying reinforcement contents.

### *3.7 Finite Element Simulation*

A finite element simulation (FEA) was carried out to validate and predict the mechanical response of the recycled polyvinyl alcohol fiber (RPA), silicon nitride fiber (SN), and reduced carbon nanoparticle (RCN) reinforced composites. The experimental material properties, including tensile strength, hardness, and elastic modulus, were integrated into the computational model to ensure accuracy [14]. The model geometry, as shown in Fig. 8, was discretized using a structured meshing approach to capture localized stress and deformation behavior under external loading conditions [21,22].

The loading scenario was applied at the central region, represented by the green arrow, while the boundary conditions were imposed on the supporting wheels and rim. The color contour map illustrates the distribution of von Mises stress across the composite structure, ranging from a minimum of 0 MPa (blue) to a maximum of 154.214 MPa (red). The simulation revealed that the highest stress concentrations occurred in the central region near the applied load and at the fiber–matrix interaction zones [4]. Meanwhile, the outer rim and wheel supports demonstrated lower stress levels, highlighting effective load transfer within the composite material system [11].

The inclusion of RCN and SN fibers improved stress distribution by reducing localized peaks, thus enhancing structural stability [8]. The observed deformation patterns confirmed that the hybrid composites resisted bending and crack propagation more effectively compared to single-reinforcement composites. These findings are consistent with the experimental results, where RPA–SN–RCN (10%) composites achieved superior tensile and hardness values. Therefore, the FEA results strongly support the experimental outcomes by demonstrating improved load-bearing capacity and structural reliability [13].

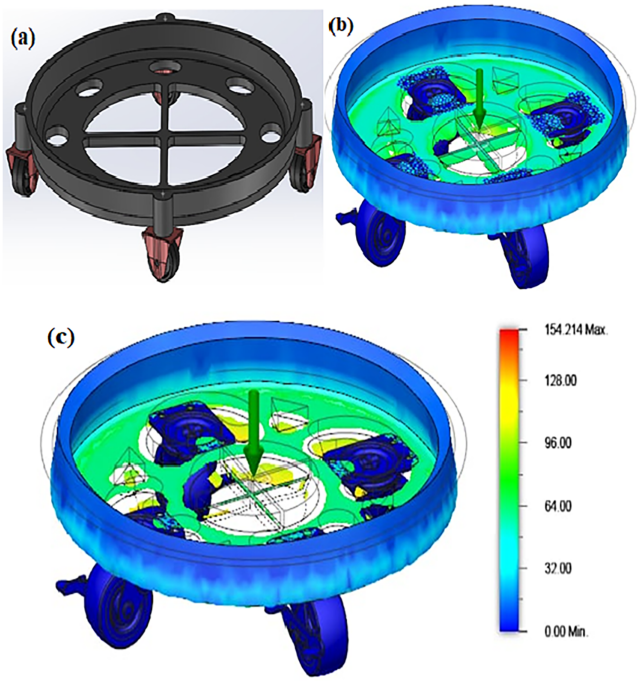


**Figure 8:** Stress contour plot (**a**–**c**) obtained from finite element analysis of RPA–SN–RCN composites under loading, showing stress concentration zones at the central region.

## 4 Conclusion

The present investigation successfully demonstrated the influence of recycled polyvinyl alcohol fiber (RPA), silicon nitride fiber (SN), and reduced carbon nanoparticles (RCN) on the microstructural development and dynamic mechanical performance of composite materials prepared by the standard dipping and silane-assisted coating process. The experimental results revealed that the inclusion of hybrid reinforcements significantly enhanced the tensile, flexural, impact, and hardness properties compared to single-reinforcement systems. Among the tested samples, the RPA–SN–RCN (10 wt%) composite exhibited the highest mechanical performance, attaining tensile strength of 62.5 MPa, flexural strength of 64.6 MPa, impact resistance of 37.5 J/m$^2$, and hardness of 88 (Shore-D). This superior performance is attributed to the synergistic effect of SN fibers and RCN particles, which contributed to strong interfacial bonding, refined microstructures, and effective crack arresting mechanisms. The microstructural observations confirmed the presence of solid phases, lattice structures, and secondary crystalline boundaries, all of which improved load transfer across the fiber–matrix interface. The gradual increase in hardness with silane-assisted surface modification also highlighted the importance of resin–silane interactions in reinforcing the outer composite layers. Comparatively, single reinforcement systems such as RPA–RCN (10 wt%) achieved modest improvements, while hybridized RPA–SN–RCN composites demonstrated clear dominance across all mechanical indices. The finite element simulation (FEA) further validated these experimental findings by predicting stress distribution and deformation behavior under applied loads. The color contour mapping revealed maximum von Mises stresses of 154.214 MPa in the central loading zone, while the hybrid composites exhibited uniform stress dispersion and reduced localized stress peaks. This indicated effective reinforcement synergy, which enhanced bending resistance and suppressed crack propagation.

Overall, the integration of RPA, SN, and RCN in optimal proportions provides a sustainable and high-performance composite system. Both experimental and simulation results confirm that the RPA–SN–RCN

(10 wt%) composite offers the best balance of strength, toughness, and hardness, making it a promising candidate for structural and functional applications.

**Acknowledgement:** The authors sincerely acknowledge the support provided by the Department of Mechanical Engineering, AAA college of Engineering and Technology, Sivakasi, Tamilnadu, India for facilitating the experimental and characterization facilities required to carry out this research work.

**Funding Statement:** This research did not receive any specific grant from funding agencies in the public, commercial, or not-for-profit sectors.

**Author Contributions:** T. Subash: Conceptualization, experimental investigation, data analysis, and manuscript preparation. M. Sekar: Supervision, methodology guidance, and critical review of the manuscript. R. Selvabharathi: Project administration, resource support, and final manuscript review. All authors reviewed and approved the final version of the manuscript.

**Availability of Data and Materials:** No datasets were generated or analyzed during the current study.

**Ethics Approval:** Not applicable.

**Conflicts of Interest:** The authors declare no conflicts of interest.

## References

1. Tao R, Wu Y, Geng J, Zhan Y, Zhao L, Li B, et al. Thermochemical recycling of waste glass fiber-reinforced polymers: a research based on experiments and quantum chemical calculations. J Anal Appl Pyrolysis. 2025;192(4):107277. doi:10.1016/j.jaap.2025.107277.
2. Xin Q, Zhang H, Zhan Z, Shao P, Zhang M. Enhancement of organic adsorption, photocatalysis, and mechanical properties in composites through modified recycled glass-fiber reinforced polymer powder. Constr Build Mater. 2025;472(17):140919. doi:10.1016/j.conbuildmat.2025.140919.
3. Gavilanes D, Valle V, Quiroz F, Cadena F, Iribarren JI. Valorizing urban pruning wastes and recycled polyethylene towards sustainable natural fiber-reinforced polymer composites. Clean Mater. 2025;16:100313. doi:10.1016/j.clema.2025.100313.
4. Omana L, John RE, Das Krishna D, Paul I, Wilson R, George J, et al. Eco-conscious electromagnetic interference shielding: mechanically robust, flexible, and recyclable PVA/Graphene composite films for next-generation applications. Next Mater. 2025;9(12):101077. doi:10.1016/j.nxmate.2025.101077.
5. Liu X, Sun T, Wang X, Huang R, Huang X, Li X, et al. Development of recyclable polyvinyl alcohol-based transparent films with enhanced UV shielding for sustainable fruit preservation packaging. Food Packag Shelf Life. 2025;50(12):101553. doi:10.1016/j.fpsl.2025.101553.
6. Song S, Ren W, Qin Y, He Z, Ji D, Wang R, et al. Recyclable polyvinyl alcohol/silvered carbon fiber composite foam with excellent electromagnetic shielding and mechanical stability. J Ind Eng Chem. 2025;148(2):838–47. doi:10.1016/j.jiec.2025.01.043.
7. Zahid M, Khan MI, Shafiq N, Abbas YM, Khatib JM. Achieving superior mechanical performance in one-part geopolymer composites through innovative hybrid fiber systems of recycled steel and PVA fibers. J Mater Res Technol. 2024;32:1772–87. doi:10.1016/j.jmrt.2024.08.002.
8. Ram P, Singh R, Sharma A. Mechanical and durability performance of recycled polyvinyl alcohol fiber reinforced composites. Constr Build Mater. 2020;252:119061. doi:10.1016/j.conbuildmat.2020.119061.
9. Sharma A, Smith JA, Kurtz MA, Derr T, DeSantis PM, Bock RM, et al. Hybrid-manufactured silicon nitride coated CFR-PEKK: a candidate biomaterial for trauma plate applications? J Mech Behav Biomed Mater. 2025;171(2):107141. doi:10.1016/j.jmbbm.2025.107141.

10. Wang T, Zhang L, Gao Q, Zhang B, Wan X, Li H, et al. Interface design of carbon fiber composites by fabricating interlocked carbon nanotubes-silicon nitride nanowires. J Mater Res Technol. 2024;29:4558–67. doi:10.1016/j.jmrt.2024.02.183.
11. Wan X, Zhang L, Zhang B, Gao Q, Wang T, Li H, et al. Elevating mechanical and biotribological properties of carbon fiber composites by constructing graphene-silicon nitride nanowires interlocking interfacial enhancement. J Materiomics. 2024;10(5):1080–90. doi:10.1016/j.jmat.2023.11.009.
12. Sun L, Zhang L, Yu H, Cui T, Ma S, Li H. Interlocked silicon nitride nanowires-vertical carbon nanotubes/hydroxyapatite networks for reinforcing PEEK polymer composites. Polymer. 2025;333(1):128668. doi:10.1016/j.polymer.2025.128668.
13. Kumar V, Rajan K, Patel R. Mechanical properties and oxidation resistance of silicon nitride fiber-reinforced ceramic composites. Ceram Int. 2019;45(12):15147–155. doi:10.1016/j.ceramint.2019.04.067.
14. Yin Y, Liu S, Wu X, Liu D, Siddique A, Umair M, et al. MOF-based interfacial phase inhibiting structural damage of carbon fiber reinforced polymer composites derived from high-energy irradiation. Compos Part B Eng. 2025;306:112817. doi:10.1016/j.compositesb.2025.112817.
15. Zhou L, Lu Y. Chloromethylated magnetic polystyrene composite nanoparticles prepared via RAFT-mediated surfactant-free emulsion polymerization. Colloids Surf A Physicochem Eng Aspects. 2024;684(12):133144. doi:10.1016/j.colsurfa.2024.133144.
16. Singh AK, Malik P, Chauhan G, Hegde G, Malik P. Synthesis and characterization of biowaste-based porous carbon nanoparticle-polymer dispersed ferroelectric liquid crystal composites. J Mol Liq. 2023;390:123024. doi:10.1016/j.molliq.2023.123024.
17. Haghgoo M, Ansari R, Hassanzadeh-Aghdam MK, Sahmani S, Jang SH. Numerical simulation of thermomagnetic carbon nanotube-graphene nanoplatelet polymeric conductive composites. Compos Part A Appl Sci Manuf. 2025;199:109217. doi:10.1016/j.compositesa.2025.109217.
18. Ali H, Ali S, Ali K, Ullah S, Ismail PM, Humayun M, et al. Impact of the nanoparticle incorporation in enhancing mechanical properties of polymers. Results Eng. 2025;27(4):106151. doi:10.1016/j.rineng.2025.106151.
19. Raja T, Devarajan Y. Study on the mechanical and thermal properties of basalt fiber-reinforced lead oxide nanoparticle polymer composite for advanced energy storage applications. J Energy Storage. 2025;108(3):115079. doi:10.1016/j.est.2024.115079.
20. Padmavathy S, Ramya G, Selvabharathi R. Effect on one-type dipping coating method of microstructure and physical properties of Indian almond fiber (IAF)/titanium oxide ($TiO_2$)/zirconium oxide ($Zr_2O_3$)/carbon nanotube (CNT) inorganic-organic nanocomposite materials. Biomass Convers Biorefin. 2024;14(24):31561–73. doi:10.1007/s13399-023-04983-3.
21. Sriram S, Singh RK, Kumar A. Silica and Silane based polymer composite coating on glass slide by dip-Coating Method. Surf Interfaces. 2020;19(6):100472. doi:10.1016/j.surfin.2020.100472.
22. Wu Y, He G, Liu M, Huang L, Xiang Y. Epoxy-functionalized coatings via free radical polymerization: spray-drying enabled interfacial engineering for high-performance SBR/Kaolin composites. Prog Org Coat. 2025;208(20):109529. doi:10.1016/j.porgcoat.2025.109529.
23. Raja GM, Vasanthanathan A, Selvabharathi R. Effect of one-step dipping coating process on microstructure and tribology of polypropylene/graphene oxide/carbon nanotube nanocomposites. Iran Polym J. 2023;32(6):739–48. doi:10.1007/s13726-023-01161-0.
24. Lee J, Park S, Kim H. Enhancement of tribological performance of polymer composites by surface coating methods. Surf Coat Technol. 2018;349(7):719–28. doi:10.1016/j.surfcoat.2018.06.078.